Published in final edited form as:

Nanotechnology. 2018 April 20; 29(16): 165101–. doi:10.1088/1361-6528/aaaf16.

Magnetic Resonance and Photoacoustic Imaging of Brain Tumors Using Carotid Artery Injection of Mesenchymal Stem Cells Labeled with a Multifunctional Nanoparticle

Yang Qiao[1,5], **Joy Gumin**[2], **Christopher J. MacLellan**[3,4], **Feng Gao**[2], **Richard Bouchard**[3,4], **Frederick F. Lang**[2], **R. Jason Stafford**[3,4], and **Marites P. Melancon**[1,4,*]

[1]Department of Interventional Radiology, The University of Texas MD Anderson Cancer Center, 1515 Holcombe Blvd., Houston, TX 77030, USA

[2]Department of Neurosurgery, The University of Texas MD Anderson Cancer Center, 1515 Holcombe Blvd., Houston, TX 77030, USA

[3]Department of Imaging Physics, The University of Texas MD Anderson Cancer Center, 1515 Holcombe Blvd., Houston, TX 77030, USA

[4]The University of Texas MD Anderson Cancer Center UTHealth Graduate School of Biomedical Sciences, 6767 Bertner Ave., Houston, TX 77225, USA

[5]Texas A&M University College of Medicine, 8447 Riverside Pkwy., Bryan, TX 77807, USA

Abstract

Objective—To evaluate the feasibility of visualizing bone marrow-derived human mesenchymal stem cells (MSCs) labeled with a gold-coated magnetic resonance (MR)-active multifunctional nanoparticle and injected via the carotid artery for assessing the extent of MSC homing in glioma-bearing mice.

Materials and Methods—Nanoparticles containing superparamagnetic iron oxide coated with gold (SPIO@Au) with a diameter of ~82 nm and maximum absorbance in the near infrared region were synthesized. Bone marrow-derived MSCs conjugated with green fluorescent protein (GFP) were successfully labeled with SPIO@Au at 4 μg/mL and injected via the internal carotid artery in 6 mice bearing orthotopic U87 tumors. Unlabeled MSCs were used as a control. The ability of SPIO@Au-loaded MSCs to be imaged using MR and photoacoustic (PA) imaging at t = 0 h, 2 h, 24 h, and 72 h was assessed using a 7-T Bruker Biospec experimental MR scanner and a Vevo LAZR PA imaging system with a 5-ns laser as the excitation source. Histological analysis of the brain tissue was performed 72 h after MSC injection using GFP fluorescence, Prussian blue staining, and hematoxylin-and-eosin staining.

Results—MSCs labeled with SPIO@Au at 4 μg/mL did not exhibit cell death or any adverse effects on differentiation or migration. The PA signal in tumors injected with SPIO@Au-loaded MSCs was clearly more enhanced post-injection, as compared with the tumors injected with unlabeled MSCs at t = 72 h. Using the same mice, T2-weighted MR imaging results taken before

*Corresponding author. Marites P. Melancon, PhD, Department of Interventional Radiology, The University of Texas MD Anderson Cancer Center, 1515 Holcombe Blvd., Unit 1471, Houston, TX 77030. Tel.: (713) 794-5387; mmelancon@mdanderson.org.

injection and at t = 2 h, 24 h, and 72 h were consistent with the PA imaging results, showing significant hypointensity of the tumor in the presence of SPIO@Au-loaded MSCs. Histological analysis also showed co-localization of GFP fluorescence and iron, thereby confirming that SPIO@Au-labeled MSCs continue to carry their nanoparticle payloads even at 72 h after injection.

Conclusions—Our results demonstrated the feasibility of tracking carotid artery-injected SPIO@Au-labeled MSCs in vivo via MR and PA imaging.

Keywords

mesenchymal stem cells; glioma; magnetic resonance imaging; photoacoustic imaging; superparamagnetic iron oxide nanoparticles; gold nanoparticles

Introduction

Mesenchymal stem cell (MSC)-mediated therapies have been revolutionizing oncology since their discovery. They have been especially transformative as novel therapies for physically sequestered, difficult-to-reach cancers, most notably the stage 4 astrocytoma glioblastoma multiforme (GBM). To date, bioengineered MSCs have been used in a variety of successful applications against GBM, for instance, to deliver chemotherapeutic drugs, antitumor proteins such as interferon-β, and suicide genes that cause bystander killing [1-7]. By following chemoattractant signals such as transforming growth factor β, platelet-derived growth factor subunit B, and vascular endothelial growth factor, MSCs can migrate into brain tumors and circumscribe both the developing tumor mass and the diffuse glioma stem cells of the glioma “border zone” [8-12]. The discovery that MSCs can home to brain tumors makes them of invaluable importance for targeting and treating GBMs, whether it is for the delivery of payloads or for the enhancement of contrast imaging.

Although intravenous (IV) injection of MSCs for the treatment of cerebral pathologies has been well studied alongside many other routes of administration, including intraventricular, intralesional, and intrathecal injection, only a few studies have tested the viability of using intra-arterial injection for MSC-mediated treatment of brain lesions [13-18]. There are many advantages to administering MSCs intra-arterially, most notably that intra-carotid artery injection provides a direct path for the migration of MSCs into the brain [19-21]. In contrast, IV injection requires MSCs to navigate peripherally—through the heart and lungs—before reaching the arterial circulation and entering the brain. This complicated route allows for many unwanted side effects, including an increase in the risk of MSC accumulation in the lungs, which can lead to iatrogenic atelectasis and an increased risk of pulmonary embolism [20, 22]. MSCs injected into the carotid artery are less likely than IV-injected MSCs to become entrapped in the lungs because their path to the brain is concurrent with the direction of blood flow. For these reasons, intra-carotid artery administration is more effective at targeting MSCs to the brain and has fewer systemic side-effects than IV administration [19-21].

One of the most promising applications of MSC-mediated therapy in the treatment of GBM is the delivery of contrast agents to the region of the brain tumor. Upon arrival of contrast agent-labeled MSCs at the region of brain injury, contrast imaging can be performed,

essentially creating a map of the localization of MSCs in the neoplastic or ischemic lesion. This application allows for precise visualization of the MSCs in the brain lesion, which is important for clinical evaluations of MSC-based therapy. One imaging technique that is currently being studied for use with contrast-labeled MSCs is magnetic resonance imaging (MRI). MSCs labeled with superparamagnetic iron oxide (SPIO) nanoparticles or gadolinium diethylenetriamine pentaacetic acid can transmit MR-detectable signals through the skull [23-26]. Notably, SPIO-loaded MSCs have demonstrated quantitatively measurable MR sensitivity as they migrate to and circumscribe the developing GBM [3, 26-29].

Although MRI has been previously studied for the mapping of GBM, there is little information in the literature regarding the use of photoacoustic (PA) imaging with contrast-labeled MSCs for mapping brain tumors. PA imaging is a higher-resolution alternative to MRI that uses light pulses (or “chirps”) to excite molecular contrast agents, which generate ultrasonic waves detectable by a transducer, creating a 3-dimensional image of the region of interest [30-33]. Despite the advantages of MRI for basic monitoring of MSC-mediated therapy, its low resolution, high cost, and immobile setup diminish its viability for dynamic intra-operative use. In contrast, PA imaging uses a high-resolution, low-cost, portable device that can be used multiple times intra-operatively for real-time 3-dimensional monitoring of gold nanoparticle-labeled MSCs [30-33]. Additionally, encapsulation of SPIO with gold creates a nanoparticle (SPIO@Au) capable of detection by both PA and MR imaging [30, 34-35]. The core-shell structure of this nanoparticle gives it its dual-modality activity: the SPIO in the core renders the nanoparticle MR-active, while the gold shell makes it detectable by PA imaging. In this study, we labeled MSCs with an optimal concentration of a multifunctional SPIO@Au nanoparticle to test whether this method is feasible for use in real-time monitoring of MSC-mediated therapy delivered via carotid artery injection.

Materials and Methods

Materials

Tetrakis(hydromethyl)phosphonium chloride (THPC), chloroauric acid ($HAuCl_4$), ethanol, ammonium hydroxide, tetraethyl-orthosilicate (TEOS), 3-aminopropyltrimethyloxysilane (APTMS), potassium carbonate (K_2CO_3), polyvinylpyrrolidone (PVP), and O-[2-(3-mercaptopropionylamino)ethyl]-O′-methylpolyethylene glycol (amino-functionalized methyl-PEG) were purchased from Sigma Aldrich (St. Louis, MO). Formaldehyde was purchased from EM Science (White House Station, NJ). Water-based SPIO nanoparticles (EMG 304) were purchased from Ferrotec USA (Nashua, NH).

Synthesis of SPIO@Au Nanoparticles

The SPIO@Au nanoparticles were synthesized using the method described by Ji et al. [34]. SPIO nanoparticles of about 10 nm in diameter were coated with silica using the gel-sol method and then seeded with gold to create a center of nucleation for future auric coating. Next, a potassium chloroaurate solution (K-Au) was prepared by mixing 2 mL of 1% (wt) H_4AuCl_4 with 100 mL water containing 0.025 g potassium carbonate. Potassium chloroaurate was then introduced to the silicated nanoparticles at a relative concentration of 10:1 (K-Au:THPC-SPIO@Au) with formaldehyde as the catalyst to promote the synthesis

of a complete gold monolayer over the nanoparticle. PVP was added for stabilization, and the stabilized nanoparticles were centrifuged at 6000 rpm for 10 min to obtain a pellet. The supernatant was then removed, and the pellet was resuspended for further stabilization in a 1-mL solution containing 2 mg/mL of amino-functionalized methyl-PEG (SPIO@Au-PEG). The SPIO@Au-PEG solution was rotated at room temperature overnight to facilitate full synthesis of the end product, SPIO@Au nanoparticles. The next day, the SPIO@Au nanoparticles were washed 3 times via centrifugation at 8000 rpm for 10 min, then resuspended in deionized water. The purified nanoparticles were resuspended in a final solution of 2 mL deionized water and stored at 4°C.

Characterization of SPIO@Au Nanoparticles

The average diameter of the synthesized SPIO@Au nanoparticles was measured using a transmission electron microscope (TEM) (JEOL 2010, JEOL Ltd., Tokyo, Japan) at an accelerating voltage of 80 kV. For sample analysis, a drop of the sample solution containing the SPIO@Au nanoparticles was placed on a 400-mesh copper grid and left to dry. The particle size in solution was determined using dynamic light scattering at a scatter angle of 90° on a ZetaPLUS particle size analyzer (Brookhaven Instruments Corp., Holtsville, NY).

The absorption of the SPIO@Au nanoparticles was determined using an ultraviolet (UV)-visible absorption spectrophotometer (Cary60 UV-Vis, Agilent Technologies, Santa Clara, CA), with a 1.0-cm-optical-path-length quartz cuvette.

Preparation and Labeling of Human MSCs

Male human MSCs were obtained from Lonza (Walkersville, MD). The cells were expanded in alpha minimum essential medium (α-MEM) containing 10% fetal bovine serum (FBS) (Sigma Aldrich), 1% 2 mM L-glutamine (Invitrogen, Carlsbad, CA), and 1% penicillin-streptomycin (Lonza) in an incubator at 37°C in an atmosphere of 5% CO_2. The cells were used at passages 5 to 7.

The MSCs were transduced with green fluorescent protein (GFP) using a replication-incompetent Ad5/F35-CMV-GFP vector (Vector Development Laboratory, Baylor College of Medicine, Houston, TX) [21, 36]. Monolayers were treated at a multiplicity of infection of 50 in 3 mL serum-free MSC-medium and shaken every 10 min at 37°C. After 1 h, MSC-medium containing 10% FBS was added.

To label the GFP-positive MSCs with nanoparticles, 0.5×10^6 cells were cultured without serum for 1 h and then incubated with different concentrations of SPIO@Au (1-10 μg/mL) with or without 0.1% of the transfecting agent lipofectamine (Invitrogen) for 4 h. Cells were stained with Prussian blue and examined using bright-field microscopy to qualitatively confirm cellular uptake of the nanoparticles.

In Vitro Cell Viability Assay

At the optimal concentration of labeling, the viability of cells over time was also investigated (t = 4, 24, and 72 h after labeling). The viability of labeled cells was determined by seeding 2.5×10^3 cells in 100 μL of alpha minimum essential medium (α-MEM)

containing 10% fetal bovine serum (FBS) (Sigma Aldrich), 1% 2 mM L-glutamine (Invitrogen, Carlsbad, CA), and 1% penicillin-streptomycin (Lonza) per well in a 96-well microtiter plate overnight in an incubator at 37°C in an atmosphere of 5% CO_2. The medium was aspirated on the next day, and then 100 μL of 1:10 concentration Cell Titer 96 AQ_{ueous} One Solution cell proliferation assay reagent (Promega, Madison, WI) in α-MEM without phenol red was added to each well. Cells were incubated for 1 h at 37°C in 5% CO_2, and then UV absorbance readings were taken using a VersaMax tunable microplate reader (Molecular Devices, Sunnyvale, CA) to compare cell viability in nanoparticle-labeled and unlabeled MSCs.

In Vitro Migration Assay

The migration potential of labeled MSCs was determined as previously described [37]. Briefly, 1×10^6 U87 GBM cells were cultured in 10 mL of serum-free medium for 48 h. The resulting conditioned medium was collected, centrifuged, filtered, and placed in the lower well of 24-mm Transwell tissue culture plates (Corning Inc., Corning, NY; 8-μm pore). The upper well of the Transwell plates was coated with Matrigel (BD Biosciences, San Jose, CA; 0.7 mg/mL in MEM-nonessential amino acid) and plated with either SPIO@AuNP-labeled or unlabeled MSCs (1×10^5) in 1 mL of serum-free medium. After 48 h of incubation, the migration of the MSCs through the Matrigel was determined by fixing the membrane, staining the cells using a Hema3 staining kit (Fisher Diagnostics, Middletown, VA), directly counting the number of migrated cells in 10 high-power fields (×400), and calculating the average number of cells that had migrated.

Differentiation of MSCs After Transfection

Pluripotency was tested in vitro to confirm the ability of labeled MSCs to undergo the 3 different fates of stem cell differentiation. Labeled and unlabeled MSCs were seeded at 1×10^4, 5×10^3, and 1.6×10^7 cells/cm^2 to test their ability to undergo adipogenesis, chondrogenesis, and osteogenesis, respectively, using a STEMPRO adipocyte/chondrocyte/osteocyte differentiation kit (Gibco, Grand Island, NY). Cells were allowed to attach for 2 h in complete Dulbecco's modified Eagle medium, which was then replaced with prewarmed differentiation medium. The cells were then cultured at 37°C in an atmosphere of 5% CO_2 with the differentiation medium refreshed every 3 days. Cell culture was stopped after 14 days to determine adipogenicity and chondrogenicity and at 21 days for determination of osteogenicity.

All cell monolayers were washed with phosphate-buffered saline (PBS) and fixed with 4% formaldehyde for 30 min. Cells being tested for adipogenesis were then rinsed with PBS and 60% isopropanol, stained with Oil Red O (which selectively stains lipid vesicles) for 15 min, rinsed again with 60% isopropanol, and finally rinsed in deionized water. Cells being tested for chondrogenesis were rinsed with PBS, stained with 1% Alcian blue (which selectively stains mucopolysaccharides and glycosaminoglycans) for 30 min, rinsed with 0.1 N HCl, and finally rinsed with deionized water. Cells being tested for osteogenesis were rinsed with deionized water, stained with 2% Alizarin red (which selectively stains basic calcium phosphate crystals) for 3 min, and rinsed again with deionized water. Staining patterns in MSCs with and without SPIO@Au labeling were compared.

Cerebral Inoculation of U87 Glioblastoma in Nude Mice (nu/nu)

All animal studies were approved by the Animal Care and Use Committee and conducted in accordance with the institutional guidelines of The University of Texas MD Anderson Cancer Center. All studies used male athymic nude mice (NU/NU). U87 cells, the most common and well-established glioma-forming cell line, were purchased from ATCC (Manassas, VA) and authenticated using short tandem analysis DNA fingerprinting by the Characterized Cell Line Core Facility at MD Anderson in 2012. U87 cells were cultured at 37°C in 5% CO_2 in α-MEM with 10% FBS and 1% penicillin/streptomycin.

For injection into the mice, monolayers of U87 cells were trypsinized, washed, and resuspended in PBS at a concentration of 1×10^5 cells/μL. The mice were anesthetized with ketamine/xylazine during the procedure. Inoculation of tumor cells in the brain was performed via the guide-screw method described by Lal et al. [38]. Briefly, a drill hole was made at a point 2.5 mm lateral and 1 mm anterior to the bregma. This point was chosen because it is located directly above the caudate nucleus, which has been shown to be a highly reliable intracranial site for tumor engraftment [39,40]. Five microliters of U87 cells at a concentration of 5×10^5 cells were injected via a multiport microinfusion syringe pump (Harvard Apparatus, Holliston, MA) to promote uniformity of xenograft growth. GBMs were allowed a growth period of 1 week.

Injection of SPIO@Au-labeled MSCs

Labeled and unlabeled control MSCs were trypsinized, washed, and resuspended in complete α-MEM at a concentration of 1×10^4 cells/μL and placed on ice until ready for injection. Mice with right cerebral hemisphere U87 tumors were anesthetized with isoflurane and prepared for surgery. The method used for internal carotid artery injection was that described by Fidler et al. [41] with modifications. Using a dissecting microscope, the right common carotid artery was identified and bifurcated to isolate the right internal and external carotid arteries. The proximal portion of the common carotid artery and the right external carotid artery were manually tied to ensure unidirectional flow of MSCs during injection. A 30-gauge needle was used to inject 1×10^6 cells into the distal portion of the common carotid artery. The internal carotid artery was then loosely tied above the injection site to prevent back-flow of cells, while the common carotid and right external carotid arteries were untied to allow for blood and MSC flow to the brain. Intratumoral injections were also performed under the same parameters in a second cohort of identical mice using the guide-screw method described by Lal et al. [38] for visualization of co-localizing iron and GFP signals in the brain to confirm that SPIO@Au-labeled MSCs continue to carry their nanoparticle payloads even at 72 h after injection. A small incision was made on the scalp to expose the guide screw, and 1×10^6 cells were injected using a multiport microinfusion syringe pump (Harvard Apparatus) to promote uniformity.

MRI

Prior to imaging, mice were anesthetized with 2% isoflurane gas in oxygen. Four nude mice with U87 glioma tumors were injected with SPIO@Au-loaded MSCs via the internal carotid artery, while 2 mice were injected with control MSCs. Precontrast T2-weighted images were obtained at t = 0 h, and postinjection images were taken at t = 2 h, 24 h, and 72 h using a 7-T

BioSpec experimental MRI scanner (Bruker, Bellerica, MA) equipped with 6-cm inner-diameter gradients and a 3.5-cm inner-diameter linear volume resonator. MRI was performed at the Small Animal Imaging Facility of MD Anderson Cancer Center. Axial images of the brain were acquired using a multislice RARE sequence with T2 weighting (repetition time/echo time, 3000 ms/57 ms; number of echoes, 12; signal average, 6; bandwidth, 101 kHz; MTX, 256 × 192; field of view, 4 cm × 3 cm; slice thickness, 0.75 mm).

PA Imaging

Prior to PA imaging, mice were anesthetized with 2% isoflurane gas in oxygen. Four nude mice with orthotopic U87 glioma tumors were injected with SPIO@Au-labeled MSCs via the internal carotid artery, while 2 mice were injected with unlabeled control MSCs. At 72 h after MSC injection, background images of the GBM in the brain were acquired with B-mode ultrasonography using a 21-MHz transducer. PA images of the MSCs were taken using a Vevo LAZR ultrasonic photoacoustic imaging system (FUJIFILM VisualSonics, Inc., Toronto, Canada) after excitation with a near-infrared laser with a wavelength of 810 nm. The reported PA signal values were obtained by averaging all PA intensity values above the system-noise threshold within a defined region of interest.

Histology

Mice were anesthetized with isoflurane and euthanized via intracardiac perfusion of the left ventricle with PBS and 4% paraformaldehyde 72 h following intratumoral injection of SPIO@Au-labeled and unlabeled MSCs. The mouse brains were extracted, fixed in 10% formalin, embedded in paraffin, sectioned into 5-μm slices, and placed onto slides. The slides were treated with hematoxylin and eosin and Prussian blue for visualization of the cellular contours and SPIO@Au nanoparticles, respectively. Unstained slides were used for visualization of GFP fluorescence.

Results

Synthesis and Characterization of SPIO@Au Nanoparticles

The synthesized SPIO@Au nanoparticles were characterized by a core region composed of a SPIO-silica composite surrounded by a gold outer shell. TEM images showed SPIO nanoparticles averaging 10 nm in diameter dispersed within a spherical silica matrix (Figures 1A and 1C). The outside of the SPIO-silica composite was coated with gold nanoparticles averaging 7 nm in diameter in a noncontinuous shell. Dynamic light scattering analysis showed the average diameter of the SPIO@Au nanoparticles to be around 82 nm, with a hydrodynamic volume of between 75 and 110 nm (Figure 1B). Qualitative support for these findings was provided by TEM images (Figure 1C). Analysis of the UV-visible spectra demonstrated that SPIO@Au displayed strong plasmon absorption at 810 nm, corresponding to the near-infrared (NIR) region (Figure 1D). The strong absorption of light in this region allows SPIO@Au nanoparticles to be activated by NIR radiation and detected by PA imaging (Figure 1E).

Viability, Migration, and Differentiation of SPIO@Au-labeled MSCs

Bright-field images of MSCs stained with Prussian blue iron stain confirmed that SPIO@Au nanoparticles were successfully loaded into MSCs (Figures 2A-2E). Increasing the amount of SPIO@Au (from 0 to 10 μg/mL) led to a corresponding increase in the amount of nanoparticles loaded into the MSCs. Use of 0.1% lipofectamine transfecting agent (TA) further visibly increased the amount of SPIO@Au uptake (Figure 2E). Additionally, cell viability was not compromised by increasing the amount of SPIO@Au or by adding lipofectamine during incubation (Figure 2F). We also investigated the viability of MSCs labeled with 4 μg/mL SPIO@Au over time and found that the doubling rate at which labeled cells grew was significantly lower than that of unlabeled cells, although labeled cells remained viable. Treatment with lipofectamine decreased cell proliferation further (Figure 2G). Although lipofectamine improved the transfection of SPIO@Au, we did not use lipofectamine-treated MSCs in subsequent experiments because it decreased the viability of transfected cells over time. We found no significant differences in the migration ability of labeled and unlabeled cells ($p = 0.16$) (Figure 2H).

The differentiation capacity of MSCs was not altered by SPIO@Au labeling (Figure 3). Specifically, MSCs labeled with SPIO@Au displayed Oil Red O-stained adipose vesicles (Figure 3D), Alcian blue-stained proteoglycans (Figure 3E), and Alizarin red-stained glycoproteins (Figure 3F), indicating that labeled cells retained pluripotency for adipogenesis, chondrogenesis, and osteogenesis, respectively.

In vivo T2-weighted MRI and PA Imaging

Figure 4 shows T2-weighted MR images of a representative mouse brain bearing a U87 tumor before and after intra-carotid artery injection of SPIO@Au-labeled MSCs. Progressive hypointensity of the tumor with time was clearly visualized from $t = 0$ h to $t = 72$ h. In contrast, tumors in mice injected with unlabeled MSCs did not show this progressive hypointensity over time. Quantitative signal-to-noise ratio analysis comparing the region of the tumor to the parenchyma-matched area in the contralateral brain further confirmed tumor hypointensity in mice injected with labeled MSCs.

The PA imaging map of U87 tumors 72 h after intra-carotid artery injection of SPIO@Au-labeled MSCs and unlabeled control MSCs is shown in Figure 5. At $t = 72$ h, the PA signal (using an NIR laser with excitement at 810 nm) in mice injected with labeled MSCs was 2.6 times the preinjection signal (Figure 5, right). Mice injected with unlabeled MSCs exhibited no increase in signal enhancement from baseline to 72 h (Figure 5, left). The yellow arrows in the B-mode ultrasonography images indicate where the bolt was placed when the U87 glioma cells were inoculated. Because of imaging depth limitations, the PA signal enhancement appears to correlate with the tumor-cell-containing bolt track and the most proximal aspect of the tumor, while regions of hypointensity on MRI appear to correlate more closely with the deeper-lying lesion as a whole.

Histology

Histological analysis of slides from the intratumoral injection study showed that GFP-conjugated MSCs were co-localized with the Prussian blue-stained SPIO@Au nanoparticles

within the tumor 72 h after injection. GFP fluorescence was measured using a fluorescein isothiocyanate filter. To further ensure the integrity and specificity of the GFP signal, background fluorescence was measured using tetramethylrhodamine and subtracted from the gross fluorescein isothiocyanate fluorescence measurement. Prussian blue staining revealed the presence of SPIO@Au in the location within the brain tumor corresponding to the GFP fluorescence signal indicative of MSCs (Figure 6, top). No co-localization of the 2 signals was seen in control MSCs (Figure 6, bottom). These results confirm that SPIO@Au-labeled MSCs continue to carry their nanoparticle payloads even at 72 h after injection.

Discussion

This study demonstrates that PA imaging, in conjunction with MRI, is potentially useful for planning and real-time monitoring during stem cell-mediated therapy for brain tumors. Our results show that MSCs labeled with an optimal concentration of the multifunctional nanoparticle SPIO@Au and injected into the internal carotid artery of mice bearing U87 tumors were able to localize to brain tumors and provide both PA and MR images co-localized with tumor cells, as validated by histologic examination.

We previously demonstrated that SPIO@Au nanoparticles efficiently labeled adipose-derived stem cells isolated from pigs [42] and that its optimal labeling concentration was similar to the optimal concentration used for human bone marrow-derived MSCs. Stem cells labeled with 4 μg/mL of SPIO@Au with and without lipofectamine demonstrated sufficient uptake of nanoparticles. However, because lipofectamine significantly reduced cell proliferation, we did not use it in subsequent experiments. At a higher concentration of 10 μg/mL, cell viability decreased by about 10%, and at lower concentrations of 1 μg/mL and 2 μg/mL, the amount of SPIO@Au was deemed insufficient. Thus, we used 4 μg/mL SPIO@Au without lipofectamine in the subsequent in vitro and in vivo studies.

MSCs labeled with 4 μg/mL of SPIO@Au also exhibited full retention of pluripotency; they were able to undergo adipogenesis, chondrogenesis, and osteogenesis. Cellular mobility at this labeling concentration was also preserved, as demonstrated by a migration assay.

Numerous studies indicate that magnetically labeled MSCs can be successfully tracked using MRI [43]. Our previous results showed that SPIO@Au nanoparticles were able to infiltrate liver fibroses following laser ablation [42]. Here, in vivo T2-weighted imaging of U87 tumors showed a clear difference between the precontrast images of the brain and those taken after carotid artery injection of SPIO@Au-labeled MSCs. The marked progressive hypointensity of the tumor over 72 h after injection corresponded to the localization of SPIO@Au-labeled MSCs into the tumor. Alternatively, in mice injected with control unlabeled MSCs, MR images of the tumor remained isointense before and after injection. Although the hypointensity was evident in SPIO@Au-injected tumor images, the MR images gave only a rough location of the tumor and were unable to delineate the tumor margins, where infiltrative tumors reside. PA imaging at t = 72 h also showed a significant 2.6 times increase in signal enhancement in mice injected with SPIO@Au-labeled MSCs compared with those injected with control MSCs, which did not show a significant increase in signal enhancement from baseline after 72 h. Used in conjunction, PA and MR imaging

constitute a comprehensive method for tracking MSCs in real time during stem cell-mediated drug delivery or surgery, which would aid in planning and treatment monitoring.

Although the idea of using MRI and PA imaging in conjunction has been previously tested by another group [30], the route of administration used in that study was mainly IV. Recent studies have demonstrated unfavorable biodistribution of IV-administered stem cells, finding significant numbers of transplanted cells in organs other than the brain and citing passage through the lungs as an obstacle preventing transplanted cells from reaching the diseased brain [44-47]. Penharkar et al. [49] demonstrated that intra-arterial delivery allows a significantly larger number of neural stem cells to reach the ischemic brain than does the IV route. Thus, the route of administration plays an important role in the localization and, therefore, the efficacy of the imaging. Our study confirmed that we can deliver MSCs carrying the dual-modality, multifunctional SPIO@Au nanoparticle into the brain via intra-carotid artery injection.

Conclusion

In conclusion, our data establish that intra-carotid artery injection of MSCs labeled with nanoparticles is a promising, minimally invasive route of introduction for stem cell-based therapies. By using a dual-modality, multifunctional nanoparticle, we were also able to show proof-of-concept that PA imaging can be used in conjunction with MRI for planning and realtime monitoring during stem cell-mediated therapy. The presence of gold on the nanoparticle surface also makes it possible to use laser ablation to kill cancer cells. Our previous publications on the SPIO@Au nanoparticle show that this nanoparticle can be delivered specifically to tumor cells and can also be heated by lasers for photothermal ablation therapy [35, 41]. Further in vitro and in vivo studies need to be performed to confirm whether MSCs labeled with SPIO@Au can serve as a laser ablation-mediating agent.

Acknowledgments

This research was supported in part by a National Institutes of Health - National Cancer Institute SPORE in Brain Cancer Career Development Award to M.P.M. (C2 P50 CA127001-08); a Cancer Center Support Grant (P30 CA016672) for the support of MD Anderson Cancer Center's Small Animal Imaging, Veterinary Pathology, and High Resolution Electron Microscopy core facilities; and a Shared Instrumentation Grant (S10 OD010403). C.J.M. received stipend support from the National Center for Advancing Translational Sciences of the National Institutes of Health under Award Number TL1TR000369. We thank Trevor Mitcham for running the photoacoustic imaging system and Kenneth Dunner for all the TEM imaging. We also thank Amy Ninetto for editing the manuscript.

References

1. Binello E, Germano IM. Stem cells as therapeutic vehicles for the treatment of high-grade gliomas. Neuro Oncol. 2012; 14:256–65. [PubMed: 22166262]
2. Hamada H, Kobune M, Nakamura K, Kawano Y, Kato K, Honmou O, Houkin K, Matsunaga T, Niitsu Y. Mesenchymal stem cells (MSC) as therapeutic cytoreagents for gene therapy. Cancer Sci. 2005; 96:149–56. [PubMed: 15771617]
3. Kosztowski T, Zaidi HA, Quiñones-Hinojosa A. Applications of neural and mesenchymal stem cells in the treatment of gliomas. Expert Rev Anticancer Ther. 2009; 9:597–612. [PubMed: 19445577]
4. Miletic H, et al. Bystander killing of malignant glioma by bone marrow-derived tumor-infiltrating progenitor cells expressing a suicide gene. Mol Ther. 2007; 15:1373–81. [PubMed: 17457322]

5. Nakamizo A, et al. Human bone marrow-derived mesenchymal stem cells in the treatment of gliomas. Cancer Res. 2005; 65:3307–18. [PubMed: 15833864]
6. Nakamura K, Ito Y, Kawano Y, Kurozumi K, Kobune M, Tsuda H, Bizen A, Honmou O, Niitsu Y, Hamada H. Antitumor effect of genetically engineered mesenchymal stem cells in a rat glioma model. Gene Ther. 2004; 11:1155–64. [PubMed: 15141157]
7. Sasportas LS, Kasmieh R, Wakimoto H, Hingtgen S, van de Water JA, Mohapatra G, Figueiredo JL, Martuza RL, Weissleder R, Shah K. Assessment of therapeutic efficacy and fate of engineered human mesenchymal stem cells for cancer therapy. Proc Natl Acad Sci U S A. 2009; 106:4822–27. [PubMed: 19264968]
8. Bruna A, et al. High TGFβ-Smad activity confers poor prognosis in glioma patients and promotes cell proliferation depending on the methylation of the PDGF-B gene. Cancer Cell. 2007; 11:147–60. [PubMed: 17292826]
9. Ikushima H, Todo T, Ino Y, Takahashi M, Miyazawa K, Miyazono K. Autocrine TGF-β signaling maintains tumorigenicity of glioma-initiating cells through Sry-related HMG-box factors. Cell Stem Cell. 2009; 5:504–14. [PubMed: 19896441]
10. Pohlers D, Brenmoehl J, Löffler I, Müller CK, Leipner C, Schultze-Mosgau S, Stallmach A, Kinne RW, Wolf G. TGF-β and fibrosis in different organs—molecular pathway imprints. Biochim Biophys Acta. 2009; 1792:746–56. [PubMed: 19539753]
11. Schneider T, Sailer M, Ansorge S, Firsching R, Reinhold D. Increased concentrations of transforming growth factor β1 and β2 in the plasma of patients with glioblastoma. J Neurooncol. 2006; 79:61–5. [PubMed: 16614941]
12. Shinojima N, et al. TGF-β mediates homing of bone marrow-derived human mesenchymal stem cells to glioma stem cells. Cancer Res. 2013; 73:2333–44. [PubMed: 23365134]
13. Ahn SY, Chang YS, Sung DK, Sung SI, Yoo HS, Im GH, Choi SJ, Park WS. Optimal route for mesenchymal stem cells transplantation after severe intraventricular hemorrhage in newborn rats. PLoS One. 2015; 10:e0132919. [PubMed: 26208299]
14. Karussis D, et al. Safety and immunological effects of mesenchymal stem cell transplantation in patients with multiple sclerosis and amyotrophic lateral sclerosis. Arch Neurol. 2010; 67:1187–94. [PubMed: 20937945]
15. Kim JW, Ha KY, Molon JN, Kim YH. Bone marrow-derived mesenchymal stem cell transplantation for chronic spinal cord injury in rats: comparative study between intralesional and intravenous transplantation. Spine (Phila Pa 1976). 2013; 38:E1065–74. [PubMed: 23629485]
16. Lim JY, Jeong CH, Jun JA, Kim SM, Ryu CH, Hou Y, Oh W, Chang JW, Jeun SS. Therapeutic effects of human umbilical cord blood-derived mesenchymal stem cells after intrathecal administration by lumbar puncture in a rat model of cerebral ischemia. Stem Cell Res Ther. 2011; 2:38. [PubMed: 21939558]
17. Omori Y, Honmou O, Harada K, Suzuki J, Houkin K, Kocsis JD. Optimization of a therapeutic protocol for intravenous injection of human mesenchymal stem cells after cerebral ischemia in adult rats. Brain Res. 2008; 1236:30–8. [PubMed: 18722359]
18. Studeny M, Marini FC, Dembinski JL, Zompetta C, Cabreira-Hansen M, Bekele BN, Champlin RE, Andreeff M. Mesenchymal stem cells: potential precursors for tumor stroma and targeted-delivery vehicles for anticancer agents. J Natl Cancer Inst. 2004; 96:1593–603. [PubMed: 15523088]
19. Ishizaka S, Horie N, Satoh K, Fukuda Y, Nishida N, Nagata I. Intra-arterial cell transplantation provides timing-dependent cell distribution and functional recovery after stroke. Stroke. 2013; 44:720–6. [PubMed: 23362081]
20. Mäkelä T, et al. Safety and biodistribution study of bone marrow-derived mesenchymal stromal cells and mononuclear cells and the impact of the administration route in an intact porcine model. Cytotherapy. 2015; 17:392–402. [PubMed: 25601140]
21. Yong RL, Shinojima N, Fueyo J, Gumin J, Vecil GG, Marini FC, Bogler O, Andreeff M, Lang FF. Human bone marrow-derived mesenchymal stem cells for intravascular delivery of oncolytic adenovirus Delta24-RGD to human gliomas. Cancer Res. 2009; 69:8932–40. [PubMed: 19920199]

22. Violatto MB, et al. Longitudinal tracking of triple labeled umbilical cord derived mesenchymal stromal cells in a mouse model of amyotrophic lateral sclerosis. Stem Cell Res. 2015; 15:243–53. [PubMed: 26177481]
23. Geng K, Yang ZX, Huang D, Yi M, Jia Y, Yan G, Cheng X, Wu R. Tracking of mesenchymal stem cells labeled with gadolinium diethylenetriamine pentaacetic acid by 7T magnetic resonance imaging in a model of cerebral ischemia. Mol Med Rep. 2015; 11:954–60. [PubMed: 25352164]
24. Ha BC, Jung J, BK Kwak. Susceptibility-weighted imaging for stem cell visualization in a rat photothrombotic cerebral infarction model. Acta Radiol. 2015; 56:219–27. [PubMed: 24574360]
25. Tan C, Shichinohe H, Abumiya T, Nakayama N, Kazumata K, Hokari M, Hamauchi S, Houkin K. Short-, middle- and long-term safety of superparamagnetic iron oxide-labeled allogeneic bone marrow stromal cell transplantation in rat model of lacunar infarction. Neuropathology. 2015; 35:197–208. [PubMed: 25376270]
26. Wu X, et al. In vivo tracking of superparamagnetic iron oxide nanoparticle-labeled mesenchymal stem cell tropism to malignant gliomas using magnetic resonance imaging. Laboratory investigation. J Neurosurg. 2008; 108:320–9. [PubMed: 18240929]
27. Anderson SA, Glod J, Arbab AS, Noel M, Ashari P, Fine HA, Frank JA. Noninvasive MR imaging of magnetically labeled stem cells to directly identify neovasculature in a glioma model. Blood. 2005; 105:420–5. [PubMed: 15331444]
28. Wang YX, Hussain SM, Krestin GP. Superparamagnetic iron oxide contrast agents: physicochemical characteristics and applications in MR imaging. Eur J Radiol. 2001; 11:2319–31.
29. Yi P, Chen G, Zhang H, Tian F, Tan B, Dai J, Wang Q, Deng Z. Magnetic resonance imaging of Fe_3O_4@SiO_2-labeled human mesenchymal stem cells in mice at 11.7 T. Biomaterials. 2013; 34:3010–9. [PubMed: 23357367]
30. Kircher MF, et al. A brain tumor molecular imaging strategy using a new triple-modality MRI-photoacoustic-Raman nanoparticle. Nat Med. 2012; 18:829–34. [PubMed: 22504484]
31. Lu W, et al. Effects of photoacoustic imaging and photothermal ablation therapy mediated by targeted hollow gold nanospheres in an orthotopic mouse xenograft model of glioma. Cancer Res. 2011; 71:6116–21. [PubMed: 21856744]
32. Zhang YS, Wang Y, Wang L, Wang Y, Cai X, Zhang C, Wang LV, Xia Y. Labeling human mesenchymal stem cells with gold nanocages for in vitro and in vivo tracking by two-photon microscopy and photoacoustic microscopy. Theranostics. 2013; 3:532–43. [PubMed: 23946820]
33. Alwi R, Telenkov S, Mandelis A, Leshuk T, Gu F, Oladepo S, Michaelian K. Silica-coated super paramagnetic iron oxide nanoparticles (SPION) as biocompatible contrast agent in biomedical photoacoustics. Biomed Opt Express. 2012; 3:2500–9. [PubMed: 23082291]
34. Ji X, et al. Bifunctional gold nanoshells with a superparamagnetic iron oxide-silica core suitable for both MR imaging and photothermal therapy. J Phys Chem C Nanometer Interfaces. 2007; 111:6245–51.
35. Melancon MP, Elliott A, Ji X, Shetty A, Yang Z, Tian M, Taylor B, Stafford RJ, Li C. Theranostics with multifunctional magnetic gold nanoshells: photothermal therapy and t2* magnetic resonance imaging. Invest Radiol. 2011; 46:132–40. [PubMed: 21150791]
36. Olmsted-Davis EA, Gugala Z, Gannon FH, Yotnda P, McAlhany RE, Lindsey RW, Davis AR. Use of a chimeric adenovirus vector enhances BMP2 production and bone formation. Hum Gene Ther. 2002; 13:1337–47. [PubMed: 12162816]
37. Hata N, Shinojima N, Gumin J, Yong R, Marini F, Andreeff M, Lang FF. Platelet-derived growth factor BB mediates the tropism of human mesenchymal stem cells for malignant gliomas. Neurosurgery. 2010; 66:144–57. [PubMed: 20023545]
38. Lal S, Lacroix M, Tofilon P, Fuller GN, Sawaya R, Lang FF. An implantable guide-screw system for brain tumor studies in small animals. J Neurosurg. 2000; 92:326–33. [PubMed: 10659021]
39. Franklin, KBJ., Paxinos, G. The Mouse Brain in Stereotaxic Coordinates. San Diego: Academic Press; 1996.
40. Kobayashi N, Allen N, Clendenon NR, Ko LW. An improved rat brain-tumor model. J Neurosurg. 1980; 53:808–15. [PubMed: 7003068]
41. Fidler IJ, Schackert G, Zhang RD, Radinsky R, Fujimaki T. The biology of melanoma brain metastasis. Cancer Metastasis Rev. 1999; 18:387–400. [PubMed: 10721492]

42. Zhao J, Vykoukal J, Abdelsalam M, Recio-Boiles A, Huang Q, Qiao Y, Singhana B, Wallace M, Avritscher R, Melancon MP. Stem cell-mediated delivery of SPIO-loaded gold nanoparticles for the theranosis of liver injury and hepatocellular carcinoma. Nanotechnology. 2014; 25:405101b. [PubMed: 25211057]

43. Berman SMC, Walczak P, Bulte JWM. Tracking stem cells using magnetic nanoparticles. Wiley Interdiscip Rev: Nanomed Nanobiotechnol. 2011; 3:343–55. [PubMed: 21472999]

44. Gao J, Dennis JE, Muzic RF, Lundberg M, Caplan AI. The dynamic in vivo distribution of bone marrow-derived mesenchymal stem cells after infusion. Cells Tissues Organs. 2001; 169:12–20. [PubMed: 11340257]

45. Aicher A, Brenner W, Zuhayra M, Badorff C, Massoudi S, Assmus B, Eckey T, Henze E, Zeiher AM, Dimmeler S. Assessment of the tissue distribution of transplanted human endothelial progenitor cells by radioactive labeling. Circulation. 2003; 107:2134–39. [PubMed: 12695305]

46. Jin K, Sun Y, Xie L, Mao XO, Childs J, Peel A, Logvinova A, Banwait S, Greenberg DA. Comparison of ischemia-directed migration of neural precursor cells after intrastriatal, intraventricular, or intravenous transplantation in the rat. Neurobiol Dis. 2005; 18:366–74. [PubMed: 15686965]

47. Fischer UM, Harting MT, Jimenez F, Monzon-Posadas WO, Xue H, Savitz SI, Laine GA, Cox CS Jr. Pulmonary passage is a major obstacle for intravenous stem cell delivery: the pulmonary first-pass effect. Stem Cells Dev. 2009; 18:683–91. [PubMed: 19099374]

48. Tarulli E, Chaudhuri JD, Gretka V, Hoyles A, Morshead CM, Stanisz GJ. Effectiveness of micron-sized superparamagnetic iron oxide particles as markers for detection of migration of bone marrow-derived mesenchymal stromal cells in a stroke model. J Magn Reson Imaging. 2013; 37:1409–18. [PubMed: 23712844]

49. Pendharkar AV, et al. Biodistribution of neural stem cells after intravascular therapy for hypoxic-ischemia. Stroke. 2010; 41:2064–70. [PubMed: 20616329]

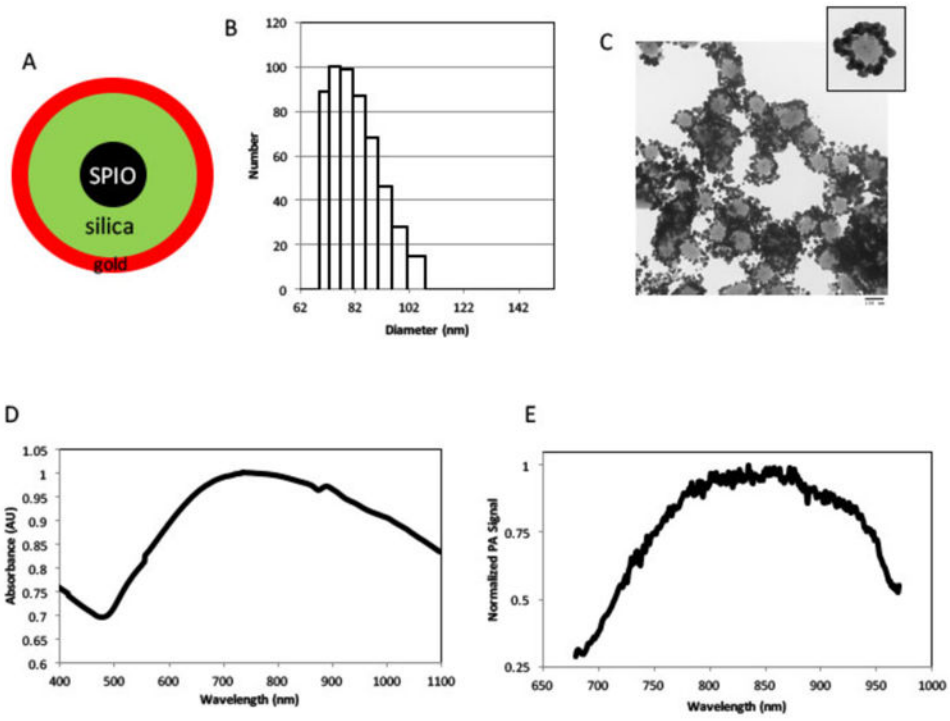

Figure 1.

Synthesis and characterization of SPIO@Au nanoparticles. (A) Schematic illustration of SPIO@Au nanoparticle containing superparamagnetic iron oxide (SPIO) core, silica, and gold coating. (B) Dynamic light scattering analysis and (C) transmission electron microscopic image of SPIO@Au indicating the size of the nanoparticle. (D) Ultraviolet-visible light absorption spectrum and (E) photoacoustic (PA) profile of SPIO@Au.

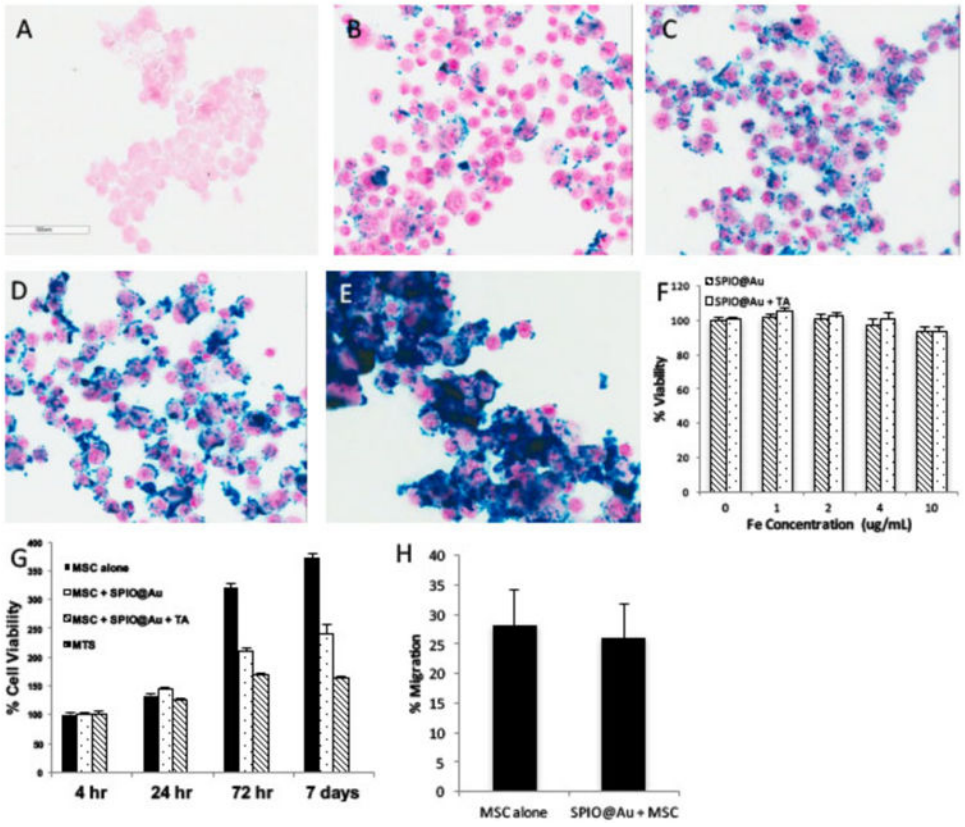

Figure 2.

In vitro characterization of SPIO@Au-labeled MSCs. (A-E) Bright-field micrographs of Prussian blue-stained MSCs loaded with different concentrations of SPIO@Au (A, no SPIO@Au; B, 1 μg/mL; C, 2 μg/mL; D, 4 μg/mL; E, 10 μg/mL + 0.1% lipofectamine). (F) Quantification of the viability of MSCs loaded with different concentrations of SPIO@Au with and without a transfecting agent (TA) at 4 h. Data are shown as means ± standard deviations (error bars). (G) Cell viability at 4 μg/mL SPIO@Au with or without 0.1% TA at different time points after MSC loading (t = 4 h, 24 h, 72 h, and 7 days). (H) Percent migration of labeled versus unlabeled MSCs ($p = 0.16$).

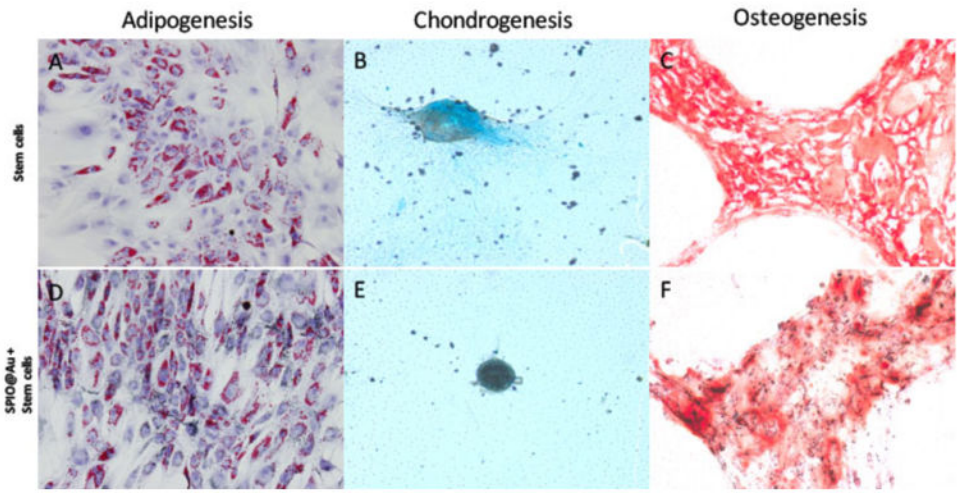

Figure 3.

Micrographs comparing the ability of MSCs with and without SPIO@Au labeling to differentiate toward adipogenic (A, D), chondrogenic (B, E), and osteogenic (C, F) lineages.

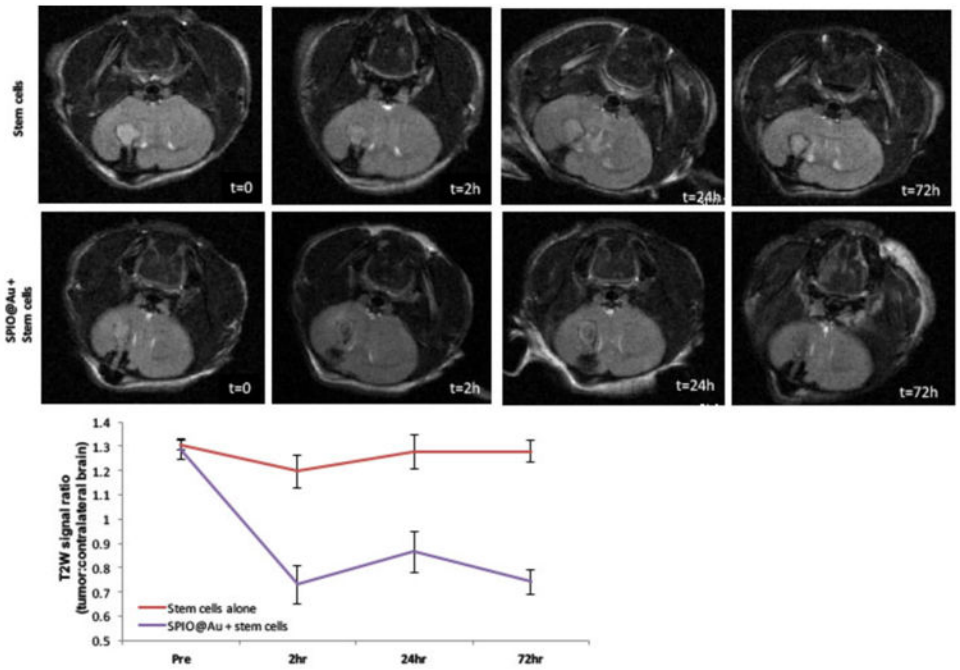

Figure 4.

Representative T2-weighted MR images of the mouse brain at various times (t = 0, 2h, 24h, and 72 h) after intra-carotid artery injection of SPIO@Au-loaded MSCs or unlabeled MSCs (top). Quantification of the T2-weighted signal of the tumor against that of the contralateral brain (bottom).

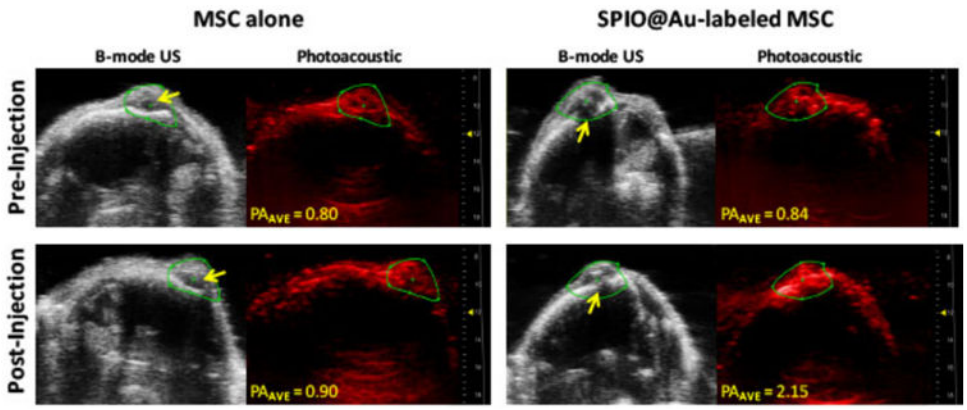

Figure 5.

In vivo photoacoustic (PA) imaging of mouse brain at 72 h after intra-carotid artery injection of SPIO@Au-labeled MSCs or MSCs alone. Yellow arrows on B-mode ultrasound (US) images of the brain indicate the bolt placement where the U87 cells were implanted into the brain. The PA images were taken at 810 nm, and the signal intensity was calculated within the green regions of interest. Average PA (PA_{AVE}) values were obtained by averaging all PA intensity values above the signal-noise threshold within the regions of interest.

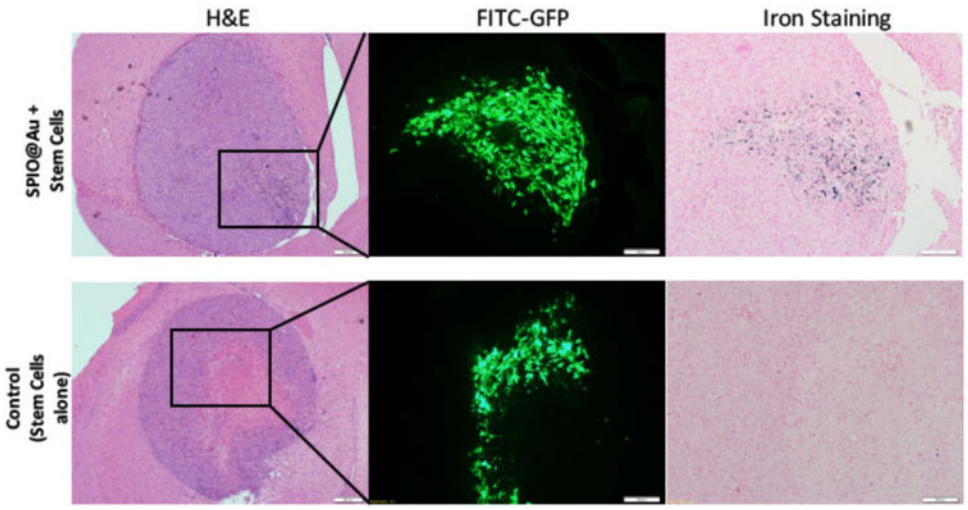

Figure 6.

Histologic analysis after intra-carotid artery injection showing SPIO@Au-loaded MSCs homing to the U87 brain tumor. Hematoxylin and eosin (H&E) staining of the mouse brain with U87 tumor (left). GFP fluorescence microscopy image at 20× magnification showing presence of MSCs (middle). Prussian blue staining of SPIO@Au indicating co-localization of the GFP-labeled MSCs and the iron of the SPIO@Au nanoparticle (right). This co-localization was not observed with the control (GFP-labeled MSCs not loaded with SPIO@Au).